

RESEARCH

Open Access



# Preoperative evaluation of microvascular invasion in hepatocellular carcinoma with a radiological feature-based nomogram: a bi-centre study

Yuhui Deng<sup>1,2†</sup>, Dawei Yang<sup>1†</sup>, Xianzheng Tan<sup>3†</sup>, Hui Xu<sup>1</sup>, Lixue Xu<sup>1</sup>, Ahong Ren<sup>1</sup>, Peng Liu<sup>3\*†</sup> and Zhenghan Yang<sup>1\*†</sup>

## Abstract

**Purpose** To develop a nomogram for preoperative assessment of microvascular invasion (MVI) in hepatocellular carcinoma (HCC) based on the radiological features of enhanced CT and to verify two imaging techniques (CT and MRI) in an external centre.

**Method** A total of 346 patients were retrospectively included (training,  $n = 185$ , CT images; external testing 1,  $n = 90$ , CT images; external testing 2,  $n = 71$ , MRI images), including 229 MVI-negative patients and 117 MVI-positive patients. The radiological features and clinical information of enhanced CT images were analysed, and the independent variables associated with MVI in HCC were determined by logistic regression analysis. Then, a nomogram prediction model was constructed. External validation was performed on CT ( $n = 90$ ) and MRI ( $n = 71$ ) images from another centre.

**Results** Among the 23 radiological and clinical features, size, arterial peritumoral enhancement (APE), tumour margin and alpha-fetoprotein (AFP) were independent influencing factors for MVI in HCC. The nomogram integrating these risk factors had a good predictive effect, with AUC, specificity and sensitivity values of 0.834 (95% CI: 0.774–0.895), 75.0% and 83.5%, respectively. The AUC values of external verification based on CT and MRI image data were 0.794 (95% CI: 0.700–0.888) and 0.883 (95% CI: 0.807–0.959), respectively. No statistical difference in AUC values among training set and testing sets was found.

**Conclusion** The proposed nomogram prediction model for MVI in HCC has high accuracy, can be used with different imaging techniques, and has good clinical applicability.

**Keywords** Hepatocellular carcinoma, Microvascular invasion, CT, MRI, Nomogram

<sup>†</sup>Peng Liu and Zhenghan Yang share the corresponding authorship of this article.

<sup>†</sup>Yuhui Deng, Dawei Yang and Xianzheng Tan contributed equally to this study.

\*Correspondence:

Peng Liu  
lpradiology@163.com  
Zhenghan Yang  
yangzhenghan@vip.163.com

Full list of author information is available at the end of the article



© The Author(s) 2024. **Open Access** This article is licensed under a Creative Commons Attribution 4.0 International License, which permits use, sharing, adaptation, distribution and reproduction in any medium or format, as long as you give appropriate credit to the original author(s) and the source, provide a link to the Creative Commons licence, and indicate if changes were made. The images or other third party material in this article are included in the article's Creative Commons licence, unless indicated otherwise in a credit line to the material. If material is not included in the article's Creative Commons licence and your intended use is not permitted by statutory regulation or exceeds the permitted use, you will need to obtain permission directly from the copyright holder. To view a copy of this licence, visit <http://creativecommons.org/licenses/by/4.0/>. The Creative Commons Public Domain Dedication waiver (<http://creativecommons.org/publicdomain/zero/1.0/>) applies to the data made available in this article, unless otherwise stated in a credit line to the data.

## Background

As a most common primary liver malignancy, hepatocellular carcinoma (HCC) is among the top three causes of tumour-linked death in the world [1, 2]. Liver transplantation and surgical excision are currently the best treatment options and have been continuously furthered recently. However, because of the high recurrence rate, the early and long-term prognoses of HCC are still not ideal even after treatment [3]. Microvascular invasion (MVI) has been proved to be an important factor in the high recurrence rate of patients with HCC after resection or transplantation [4, 5]. Wide-margin surgery for MVI of HCC has been shown to reduce postoperative recurrence [6, 7]. However, MVI is a postoperative pathological diagnosis, and a noninvasive, high-precision tool is needed to assess the presence of MVI in HCC to assist in making appropriate preoperative treatment decisions.

With the characteristics of noninvasive assessment of blood supply, water molecular diffusion restriction, hepatic function and more clearly showing morphologic changes, multiple magnetic resonance imaging (MRI) techniques have been utilized to noninvasively evaluate MVI status in HCC. A meta-analysis [8] revealed that the apparent diffusion coefficient (ADC) value alone had medium accuracy to predict MVI in HCC with a pooled sensitivity, specificity and area under the receiver operating characteristic curve (AUROC) of 0.73, 0.70, and 0.78, respectively. A diagnostic accuracy of imaging features in gadoteric acid-enhanced MRI was also assessed in another meta-analysis [9], which showed a comparable accuracy to the ADC value, with AUROCs in the range of 0.74 to 0.76. However, the use of only imaging features without the consideration of clinical indices might reduce the prediction accuracy. Recently, machine learning techniques such as radiomics or deep learning models have been used to improve the efficacy of predictive methods [10–13], which have shown better diagnostic accuracy. However, considering the requirement of specialized software, weak robustness, and unsatisfactory generalization performance interhospitally, machine learning currently remains too idealized to be extensively used, especially in clinics without the appropriate conditions to apply this novelty technique.

In practise, dynamic contrast-enhanced MRI (DCE-MRI) and contrast-enhanced CT (CE-CT) remain the most valuable techniques in the detection and diagnosis of HCC in cirrhosis. Dynamic contrast enhancement technique can capture the enhancement characteristics of tumors at different periods, which is conducive to the diagnosis and differential diagnosis of liver tumors. In addition, dynamic techniques such as perfusion CT and MRI can quantify perfusion of hepatocellular carcinoma, which is currently an important means to evaluate the

effectiveness of sorafenib therapy [14–16]. All of these can be used as a supplement to conventional imaging to guide diagnosis and treatment. Meanwhile, the recognition of imaging features on DCE-MRI or CE-CT is not challenging for radiologists and experienced surgeons. Previous studies have revealed that imaging features such as tumour margins, tumour size, tumour capsule, intra-tumoural artery, and arterial peritumoral enhancement were correlated with the status of MVI in HCC, [17–21] and these features could be well captured on DCE-MRI or CE-CT. For example, Ling et al. found rim enhancement in the arterial phase and peritumoral hypointensity in the hepatobiliary phase were independent risk factors for microvascular invasion in patients with HCC [18]. Matteo et al. found tumor dimension, nonsmooth tumor margins, peritumoral enhancement, and TTPVI, had high accuracy in the prediction of MVI in HCC [19]. And Wei et al. found capsular invasion, margins and serum AFP level were associated with MVI in HCC [20]. However, few studies among them have considered these imaging features in combination with clinical indices to build a nomogram model for the prediction of MVI and verify it in different medical centres.

Therefore, the study proposed to develop a clinically practical nomogram model based on imaging features from CE-CT and clinical indices to predict MVI in HCC and to verify its generalization on external data, including both MRI and CT data.

## Methods

The patients were included from two centres, including Hunan Provincial People's Hospital, the First Affiliated Hospital of Hunan Normal University (Centre I) and Beijing Friendship Hospital, Capital Medical University Affiliated Hospital (Centre II). This retrospective study was authorized by agency review board, waiving the requirement for informed consent.

## Patients

HCC patients who underwent hepatectomy or liver transplantation at two hospital centres and were diagnosed between January 2015 and December 2020 were considered. The inclusion criteria as follows: (1) dynamic enhanced MRI (DCE-MRI) and/or enhanced CT (CE-CT) images of the liver were obtained, including at least pre-enhanced, arterial phase, portal phase, and equilibrium phase images; (2) there was no percutaneous ethanol injection, transcatheter arterial chemoembolization or radiofrequency ablation; and (3) the pathologic status of MVI in HCC was obtained from surgical resection specimens. The exclusion criteria as follows: (1) the time point of the reinforcement stage was not accurate; (2) the interval time between CT or MRI examination and

surgery was more than one month; (3) there were significant artefacts affecting the HCC observation; and (4) multiple lesions were present. Details are provided in the flowchart in Fig. 1.

Overall, 346 consecutive patients (185 patients from Centre I and 161 patients from Centre II) were enrolled, and the CT imaging data from Centre I were set as a training cohort. The CT or MRI data of Centre II were used as the external validation cohort, in which the CT imaging data were used as trial group Testing 1 and the MRI imaging data were used as Testing 2.

**Clinical characteristics**

Clinical information and preoperative laboratory tests were obtained from our case database, including age, tumour size, aetiology of liver disease, sex, alkaline phosphatase (ALP), serum alanine aminotransferase (ALT), international normalized ratio (INR), aspartate aminotransaminase (AST), glutamyl-transpeptidase (GGT), prothrombin time (PT), serum albumin (ALB), platelet count (PLT), serum total bilirubin (TB), Child–Pugh grade, background liver, and alpha-fetoprotein (AFP).

**Image acquisition**

CE-CT scanning of the liver was performed using multiple multislice spiral CT scanners. Scan from the roof of the diaphragm to the iliac ridge. It includes plain scan, arterial stage (fluoroscopic trigger, 28~35 s), portal vein stage (70-80 s) and equilibrium stage (180 s). All patients received a non-ionic iodide contrast (300 mg of iodide per ml) at a dose of 1.5 ml (450 mg of iodide) per kg of

body weight with a flow rate of 3.0–4.0 ml/s. Detailed imaging parameters of CT are shown in Table 1.

All MRI examinations are performed on a 3.0 T scanner using 16–64 channel phased array coils. Scanning sequences include: fast spin echo T2-weighted imaging, diffusion-weighted sequences (B-values: 0 s/mm<sup>2</sup> and 800 s/mm<sup>2</sup>), (3D) gradient echo T1-weighted sequence enhanced anterior imaging, Arterial phase (AP) of 15 to 25 s, Portal venous phase (50 s), PVP), 180 s Equilibrium phase (EP). The standard dose (0.1 mmol/kg) of Gadopentetic acid (Gd-DTPA) was injected at a flow rate of 2.0 ml/s. Detailed imaging parameters of MRI are shown in Table 2.

**Pathological diagnosis of MVI in HCC**

Surgical specimens were histopathologically examined by two experienced pathologists, to whom the patient’s

**Table 1** Detailed imaging parameters of CE-CT

	Philips ICT	GE Revolution	GE Discovery CT750HD
No. of channels	256	256	256
Tube voltage (kV)	120	120	120
Tube current (mA)	420	450	450
Helical pitch	0.991	0.992	0.984
Acquisition time (s)	2–6	2–6	2–6
Section thickness (mm)	1–5	1.25–5	1–5
Intersection gap	0	0	0
Reconstruction kernel	soft tissue	standard	standard

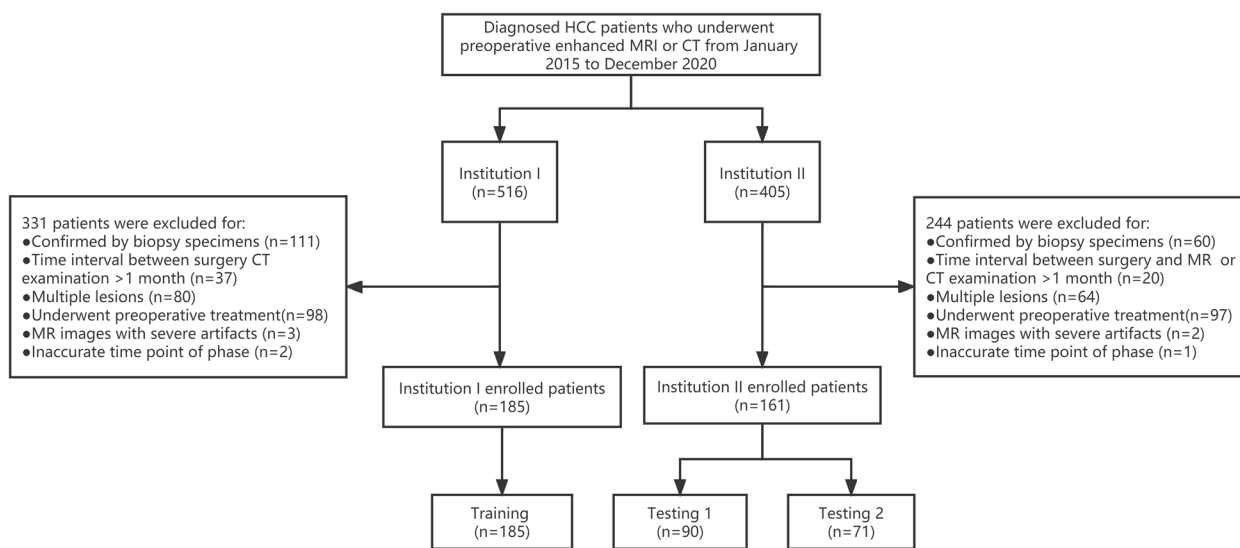


**Fig. 1** Flow Chart. HCC hepatocellular carcinoma, MRI Magnetic Resonance Imaging, CT computed tomography

**Table 2** Detailed imaging parameters of MRI

Sequence	MRI unit	TR (ms)	TE (ms)	Flip angle (°)	Matrix	FOV (mm2)
T2-weighted imaging	3.0 T Siemens Prisma	2160	100	160	320×288	433×433
	3.0 T GE Healthcare GE 750w	6315	85	150	288×244	360×280
	3.0 T Philips Ingenia	4918	106	160	288×224	285×380
Diffusion-weighted imaging	3.0 T Siemens Prisma	5600	Minimum	90	100×76	380×289
	3.0 T GE Healthcare GE 750w	3000	Minimum	90	128×128	360×380
	3.0 T Philips Ingenia	5100	55	90	128×128	285×380
Dynamic T1-weighted imaging	3.0 T Siemens Prisma	3.95	Minimum	9	352×256	400×296
	3.0 T GE Healthcare GE 750w	4.1	Minimum	15	288×172	380×300
	3.0 T Philips Ingenia	3.47	1.36	10	320×216	308×380

imaging findings and clinical history were not visible. MVI in HCC was ruled as the microscopic discovery of tumour thrombus in small peritumoral vessels, which may be hepatic veins, portal veins, or large capsular vessels aligned with the surrounding liver tissue. If there were any differences, they were resolved through consultation.

### Image analysis

All images were evaluated by two radiologists (with 10+ years of experience in abdominal imaging) with knowledge of HCC but not knowledge of the pathology associated with MVI. In the event of a disagreement over the above procedure, a third radiologist (with 15+ years of experience in abdominal imaging) helped to reach an agreement. At the same time, the Kappa value between observers was calculated, and a Kappa value greater than 0.75 was considered to indicate good repeatability.

Each patient was evaluated for the following imaging features: (1) radiological capsule, which was defined as the high-density or signal ring around the tumour in the portal phase or equilibrium phase and was classified as complete, incomplete, or absent; (2) tumour margin, which was divided into smooth and non-smooth (smooth tumour margins were defined as nodular tumours with smooth profiles in all imaging planes and vice versa); (3) arterial peritumoral enhancement (APE), which was defined as detectable enhancement near the tumour boundary in the AP, which then became equidecayed in the equilibrium phase; (4) hypoattenuating halo, which was defined as a partially or completely low-density or signal ring surrounding the tumour in the portal phase; (5) intratumoural arteries, which were defined as the internal artery presented in the arterial phase; and (6) arterial rim enhancement (ARE), which was defined on arterial phase images as irregularly rim-like peripheral hyperenhancement and a hypoenhancing area in the centre.

### Establishment and evaluation of the nomogram prediction model

First, independent predictors of MVI in HCC were identified by multiple logistic regression in clinical and radiological features. Then, a nomogram prediction model was established by thees significant factors. The degree of generalization of the model was evaluated by external validation using external centre data based on different imaging techniques. Harrell's C-index was used to evaluate the discriminability of the nomogram [22]. The nomogram diagnostic performance of the training and testing cohorts was analysed by calibration curves [23]. The consistency between the prediction of MVI and the actual MVI on the calibration curve was evaluated using the Hosmer–Lemeshow test [24]. The clinical usefulness of the nomogram was determined by decision curve analysis [25].

### Statistical analysis

Statistical analysis was performed using R software (version 3.6.1, Boston, MA, USA) and SPSS (version 26, Chicago, IL, USA). The mean ± standard deviation are used for continuous variable. The number (percentage) are used for categorical variables. Pearson's chi-square test was utilized to evaluate categorical variables, and the Mann–Whitney U test or Student's t test was utilized to evaluate continuous variables. Multivariate logistic regression analysis, nomogram prediction model construction, calibration curve, external validation, ROC curve, and decision curve ananalysis were carried out using various packages in R language. The AUC value, accuracy, sensitivity and specificity were recorded. A two-tailed *p* value lower than 0.05 was defined statistically significant.

## Results

### Demographic data

The demographic data of 346 patients from the two centres are displayed in Table 3. The mean age was 55.85 years (26–82 years). There were 280 males (47.4%) and 66 females (36.9%). There were 229 MVI-negative

**Table 3** Demographic data in the training, testing 1 and testing 2

Variable	Total (n = 346)	Training (n = 185)	Testing 1 (n = 90)	Testing 2 (n = 71)	p-Value
Age (years, mean ± SD)	55.85 ± 10.86	54.73 ± 11.21	56.53 ± 11.08	57.90 ± 9.32	0.088
Sex (n, %)					
Male	280(80.9)	155(83.8)	69(76.7)	56(78.9)	0.328
Female	66(19.1)	30(16.2)	21(23.3)	15(21.1)	
MVI status (n, %)					
Positive	117(33.8)	64(34.6)	30(33.3)	23(32.4)	0.940
Negative	229(66.2)	121(65.4)	60(66.7)	48(67.6)	

MVI microvascular invasion, SD standard deviation

cases (66.2%) and 117 MVI-positive cases (33.8%). No significant differences were found in sex, age or MVI status among the three datasets ( $p=0.088, 0.328, 0.940$ ).

### Clinical and imaging characteristics

Sixty-four of 185 lesions in the training dataset, 30 of 90 lesions in the testing 1 dataset and 23 of 71 lesions in the testing 2 dataset were confirmed to be positive for MVI by histopathology, which were based on CE-CT, CE-CT and DCE-MRI images, respectively. The general characteristics of the included cohorts are summarized in Table 4. Univariate analysis revealed that the clinical factors tumour size and serum AFP level and the imaging features tumour margins and APE were significantly correlated with MVI ( $p < 0.05$ ) in all three datasets. The imaging features additional APE in the training dataset and site and intratumoural arteries in the testing 2 dataset were significantly correlated with MVI ( $p < 0.05$ ). Tumour size (OR: 1.061; 95% CI: 1.020–1.104;  $p=0.003$ ), AFP level (OR: 2.008; 95% CI: 1.144–23.526;  $p=0.015$ ), tumour margin (OR: 2.645; 95% CI: 0.1211–5.775;  $p=0.015$ ), and APE (OR: 2.556; 95% CI: 1.085–6.021;  $p=0.032$ ) were independent predictors of MVI in multivariate analysis. From the perspective of clinical factors, the greater the AFP value is, the larger the tumour, and the greater the possibility of MVI. For the image features, MVI is more likely to appear when the tumour margins are not smooth and the tumour has APE. The Kappa values between observers were 0.832~0.876 for radiological features.

### Development and validation of the nomogram

The nomogram of MVI in HCC is presented in Fig. 2. Among the nomogram predictors, size had the highest score (100 points on the scale axis), followed by AFP, tumour margin and APE (30 points, 18 points and 16 points, respectively). The probability of MVI in HCC can be easily estimated by summing the points of the four variables and locating the corresponding score on the probability axis. The AUCs for the predictive performance of

the nomogram were 0.834 (95% CI: 0.774–0.895) in the training dataset, 0.794 (95% CI: 0.700–0.888) in the testing 1 dataset and 0.883 (95% CI: 0.807–0.959) in the testing 2 dataset (see Fig. 3), with no significant difference ( $p > 0.05$ ) (see Table 5). The calibration curves (Fig. 4) showed that in the training ( $\chi^2=5.179, p=0.738$ ), testing 1 ( $\chi^2=6.557, p=0.585$ ) and testing 2 cohorts ( $\chi^2=9.886, p=0.273$ ), the prediction probability of the nomogram was in close agreement with the actual MVI estimate. Nomogram decision curves for the training, test 1 and test 2 datasets are shown in Fig. 5. When the threshold probability is between 0.04 and 0.78 in the training, the predicted net benefits of the nomogram decision curve were higher than those assuming that all patients have MVI. This suggests that our nomogram treatment strategy will improve clinical outcomes.

### Discussion

Our study demonstrated that a combination of clinical factors, including serum AFP level and tumour size, as well as imaging features, including tumour margin and APE, can predict MVI in HCC. In addition, we established a nomogram that included AFP level, tumour size, tumour margin, and APE to predict MVI with high accuracy and was validated internally and externally. Importantly, the combination of clinical factors and radiological feature in the nomogram affords a direct, noninvasive, and robust method for the personalized prediction in MVI preoperatively.

Of the clinical factors, the results of univariate and multivariate analyses showed that serum AFP level and tumour size were both significant risk factors for MVI, which was consistent with previous reports [21, 26–28]. Serum AFP levels as a marker for HCC have been shown to be associated with factors of tumour aggressiveness including MVI and differentiation [29]. In this study, the serum AFP level was significantly related with MVI, especially when the AFP value was greater than 400 ng/ml, but the sensitivity (67.2%) and specificity (58.7%) were low. The possible reason is that AFP is not a specific

**Table 4** Clinical and radiological characteristics of all patients of Mvi (+) And Mvi (-) groups in the training, testing 1 and testing 2

	Training Cohort (n= 185)		P-Value	Testing Cohort 1 (n=90)		P-Value	Testing Cohort 2 (n=71)		P-Value	P-Value*
	MVI (-) = 121	MVI (+) = 64		MVI (-) = 60	MVI (+) = 30		MVI (-) = 48	MVI (+) = 23		
Clinical information										
Age,years	54.40 ± 11.30	55.34 ± 11.09	0.589	56.03 ± 12.72	56.78 ± 10.27	0.764	57.88 ± 10.49	57.96 ± 6.42	0.973	
Gender			0.794			0.113			0.478	
Male	102(84.3)	53(82.8)		49(81.7)	20(66.7)		39(75)	17(69.6)		
Female	19(15.7)	11(17.2)		11(18.3)	10(33.3)		9(25)	6(36.4)		
Etiology of liver disease										
HBV	106(87.6)	51(79.7)	0.224	47(78.4)	25(41.7)	0.170	34(70.8)	18(78.3)	0.749	
HCV	3(2.5)	1(1.5)		2(3.3)	3(5)		3(6.3)	3(13)		
other	12(9.9)	12(18.8)		11(18.3)	2(3.3)		11(22.9)	2(8.7)		
ALT			0.867			0.454			0.08	
<40	76(62.8)	41(64.1)		31(51.7)	18(60)		25(52.1)	17(73.9)		
>40	45(37.2)	23(35.9)		29(48.3)	12(40)		23(47.9)	6(26.1)		
AST			0.209			1			0.678	
<35	74(61.2)	33(51.6)		30(50)	15(50)		29(60.4)	15(65.2)		
>35	47(38.8)	31(48.4)		30(50)	15(50)	0.209	19(39.6)	8(34.8)	0.335	
ALP			0.372			0.209			0.335	
<135	106(86.6)	53(82.8)		49(81.7)	21(70)		45(93.8)	20(87)		
>135	15(13.4)	11(17.2)		11(18.3)	9(30)		3(6.3)	3(13)		
GGT			0.624			0.371			0.265	
<60	80(66.1)	40(62.5)		32(53.3)	13(43.3)		29(60.4)	17(73.9)		
>60	41(33.9)	24(37.5)		28(46.7)	17(56.7)		19(39.6)	6(26.1)		
ALB			0.996			0.134			0.885	
<40	70(57.9)	37(57.8)		36(60)	13(43.3)		28(58.3)	13(56.5)		
>40	51(42.1)	27(42.2)		24(40)	17(56.7)		20(41.7)	10(43.5)		
PT			0.696			0.858			0.199	
<13.5	110(90.9)	60(93.8)		47(78.3)	23(76.7)		43(89.6)	18(78.3)		
>13.5	11(9.1)	4(6.2)		13(21.7)	7(23.3)		5(10.4)	5(21.7)		
INR			0.915			0.837			0.635	
<1.2	111(91.7)	59(92.2)		51(85)	25(83.3)		42(87.5)	21(91.3)		
>1.2	10(8.3)	5(7.8)		9(15)	5(16.7)		6(12.5)	2(8.7)		
PLT			0.841			0.371			0.128	
<125	51(42.1)	26(40.6)		28(46.7)	17(56.7)		16(33.3)	12(52.2)		
>125	70(57.9)	38(59.4)		32(53.3)	13(43.3)		32(66.7)	11(47.8)		

**Table 4** (continued)

	Training Cohort (n = 185)		P-Value	Testing Cohort 1 (n = 90)		P-Value	Testing Cohort 2 (n = 71)		P-Value	P-Value*
	MVI (-) = 121	MVI (+) = 64		MVI (-) = 60	MVI (+) = 30		MVI (-) = 48	MVI (+) = 23		
TB										
<20.4	88(72.7)	50(78.1)	0.422	30(50)	17(56.7)	0.551	25(52.1)	12(52.2)	0.994	
>20.4	33(27.3)	14(21.9)		30(50)	13(43.3)		23(47.9)	11(47.8)		
Child-Pugh class			0.132			0.273			0.456	
A	89(73.6)	38(59.4)		43(71.7)	23(76.7)		39(81.3)	21(91.3)		
B	22(18.2)	19(29.7)		13(21.7)	3(10)		7(14.6)	2(8.7)		
C	10(8.3)	7(10.9)		4(6.6)	4(13.3)		2(4.1)	0(0)		
AFP			<0.001			0.004			0.01	0.015
<20	71(58.7)	22(34.4)		34(56.7)	6(20)		26(54.2)	4(17.4)		
20–400	46(38)	27(42.2)		14(23.3)	11(36.7)		15(33.3)	15(65.2)		
>400	4(3.3)	15(23.4)		12(20)	13(43.3)		7(14.6)	4(17.4)		
size	33.01 ± 10.4	43.11 ± 11.99	0.002	31.58 ± 18.84	49.30 ± 23.15	<0.001	28.27 ± 13.56	43.87 ± 14.29	<0.001	0.03
Radiological Features										
Site			0.286			0.232			0.047	
Left lobe	29(24)	20(31.3)		13(21.7)	10(33.3)		10(20.8)	10(43.5)		
Right lobe	92(76)	44(68.7)		47(78.3)	20(66.7)		38(79.2)	13(56.5)		
Cirrhosis of the liver			0.505			0.436			0.233	
no	34(28.1)	21(32.8)		12(20)	4(13.3)		14(29.2)	10(43.5)		
yes	87(71.9)	43(68.2)		48(80)	26(86.7)		34(70.8)	13(56.5)		
ARE			0.016			0.062			0.156	0.212
no-ring	117(96.7)	55(85.9)		57(95)	24(80)		46(95.8)	19(82.6)		
ring	4(3.3)	9(14.1)		3(5)	6(20)		2(4.2)	4(17.4)		
Radiological capsule			0.208			0.52			0.594	
yes	37(30.6)	14(21.9)		20(33.3)	8(26.7)		11(22.9)	4(17.4)		
no	84(69.4)	50(78.1)		40(66.7)	22(73.3)		37(71.1)	19(82.6)		
tumour margins			<0.001			0.004			0.001	0.015
smooth	85(70.2)	18(28.1)		39(65)	10(33.3)		35(72.9)	6(26.1)		
non-smooth	36(29.8)	46(71.9)		21(35)	20(66.7)		13(27.1)	17(73.9)		
internal arteries			0.437			0.111			0.021	
no	95(78.5)	47(73.4)		44(73.3)	17(56.7)		41(85.4)	14(66.7)		
yes	26(21.5)	17(25.8)		16(26.7)	13(43.3)		7(14.6)	9(33.3)		
hypoaattenuating haloes			0.208			0.255			0.126	
no	114(94.2)	57(89.1)		51(85)	28(93.3)		45(93.8)	18(78.3)		

**Table 4** (continued)

	Training Cohort (n= 185)		P-Value	Testing Cohort 1 (n = 90)		P-Value	Testing Cohort 2 (n = 71)		P-Value	P-Value*
	MVI (-) = 121	MVI (+) = 64		MVI (-) = 60	MVI (+) = 30		MVI (-) = 48	MVI (+) = 23		
yes	7(5.8)	7(10.9)		9(15)	2(6.7)		3(6.3)	5(21.7)		
APE			<0.001			0.048			<0.001	0.032
no	105(86.8)	37(57.8)		55(91.7)	23(76.7)		43(89.6)	12(52.2)		
yes	16(13.1)	27(42.2)		5(8.3)	7(23.3)		5(10.4)	11(47.8)		

MVI microvascular invasion, HBV hepatitis B virus, HCV hepatitis C virus, ALT alanine aminotransferase, AST aspartate aminotransaminase, ALP alkaline phosphatase, GGT glutamyl-transpeptidase, ALB albumin, PT prothrombin time, INR international normalized ratio, PLT platelet count, TB total bilirubin, AFP alpha-fetoprotein, AFE arterial rim enhancement, APE arterial peritumoral enhancement

\* multivariate regression analysis



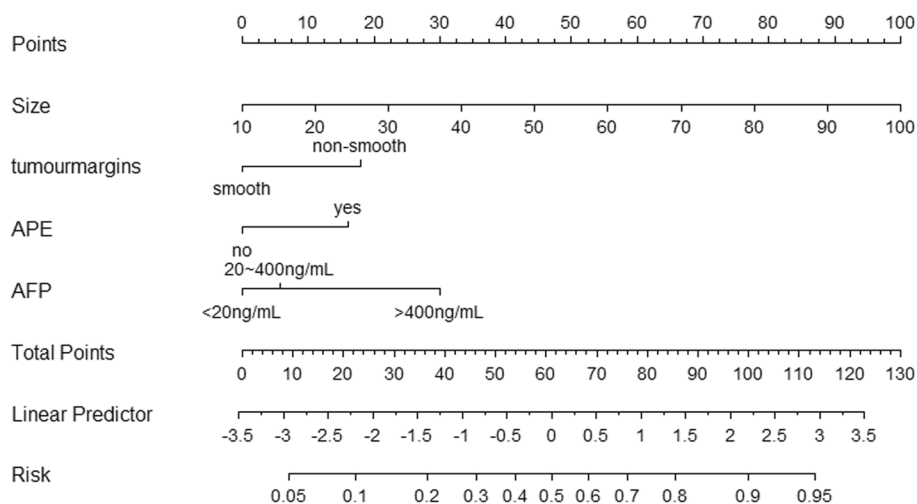


**Fig. 2** Nomogram of the model. AFP alpha-fetoprotein, APE arterial peritumoral enhancement

marker for HCC, and it can also be elevated to varying degrees in a variety of conditions, such as germ cell tumours, other gastrointestinal tumours, or cirrhosis. According to the Milan criteria, a tumour larger than 5 cm would not be suitable for liver transplantation. However, the critical value of MVI predicted by tumour size varied among studies. Shirabe et al. [30] suggested that a tumour size larger than 3.6 cm was a predictor of MVI. In another study, Kaibori et al. [31] suggested a tumour size larger than 5.0 cm as a predictor of MVI. In our study, we considered a tumour size larger than 3.15 cm to be a predictor of MVI.

Of the imaging features, the results of univariate and multivariate analyses showed that tumour margin and APE were both significant risk factors for MVI. Both tumour margin and APE are features of the peritumoral region. The area around the tumour was the most informative area, including features such as tumour-liver difference, presence or absence of hypodense halo, non-smooth margin, arterial peritumoral enhancement, and arterial rim enhancement. The tumour-liver interface may reflect cellular proliferation, MVI-induced tumour tissue distortion, extracellular matrix remodeling and the associated inflammatory response [32]. An experimental study showed that tumour margins are cross-phonemic points transmitted by the tumour to the host through transforming growth factor- $\beta$  and platelet-derived growth factor signalling and are therefore critical in tumour cells [33]. In our study, tumour margins were a strong factor in predicting MVI, with an OR value of 2.645.

In this study, we combined the above clinical and imaging features and developed a nomogram. Previous studies using radiomics and deep learning models

to predict MVI have achieved a good prediction ability, with AUCs ranging from 0.734 to 0.837 [10, 34]. However, radiomics requires much manual effort, while deep learning also requires many marker samples, and both are poorly interpretable. In clinical application, it is not as convenient and practical as our nomogram model. In addition, we performed external validation. The data in the validation dataset included both MRI and CT data. A published deep learning study revealed that an MRI-based model achieved superior prediction outcomes to a CE-CT-based model [10]. However, our study did not show a significant difference in AUC values between CT and MRI data, which indicated that our nomogram model had high applicability and generalizability and could be used on CE-CT or DCE-MRI data.

There are some limitations. First, because of the retrospective nature of this study, there may be potential selection bias. Prospective studies may be needed in the future. Second, the amount of MRI data in the validation dataset was small. Additional data may be required for separate validation in the future. Third, there is no precise evidence of a direct link between radiological features and MVI. Prospective multicentre trials are needed to further investigate the relationship between radiological features and MVI.

In conclusion, serum AFP level, tumour size, tumour margin and APE are potential biomarkers for predicting MVI in HCC patients. Combining clinical factors and imaging features, the nomogram for MVI individualized risk assessment achieves satisfactory preoperative prediction. Moreover, it can be applied to both CT and MRI data with high applicability and generalizability.

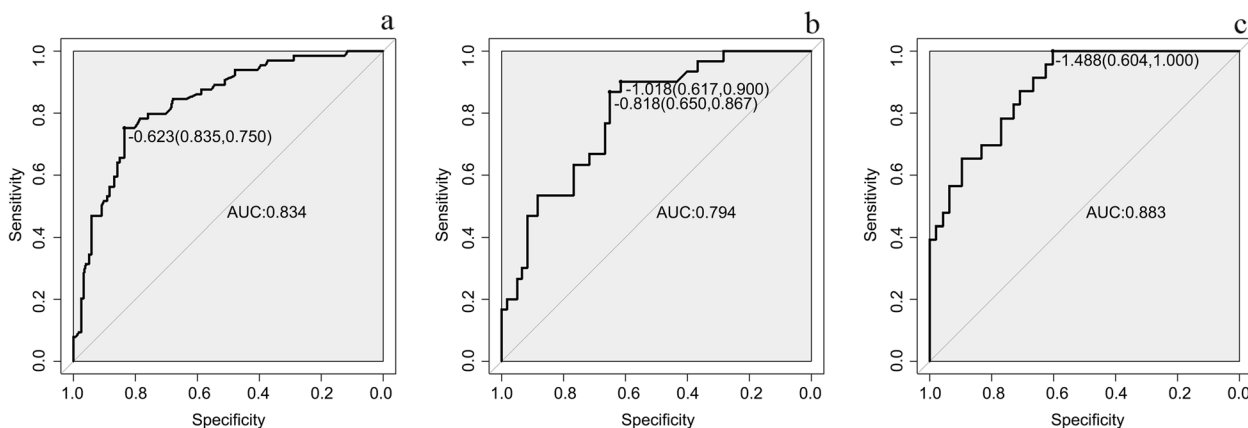


**Fig. 3** Receiver operating characteristic (ROC) curves of Training, Testing 1 and Testing 2. **a** Receiver operating characteristic (ROC) curves of Training, **b** Receiver operating characteristic (ROC) curves of Testing 1, **c** Receiver operating characteristic (ROC) curves of Testing 2

**Table 5** The diagnostic performance of nomogram model for MVI in Training, Testing 1 and Testing 2

	AUC	Accuracy	Sensitivity	Specificity	z	p
Training	0.834[0.774,0.895]	80.5	75	83.5	0.701 <sup>a</sup>	0.483
Testing 1	0.794[0.700,0.888]	71.1	90	61.7	1.143 <sup>b</sup>	0.149
Testing 2	0.883[0.807,0.959]	73.2	100	60.4	0.989 <sup>c</sup>	0.322

MVI microvascular invasion, AUC area under the receiver operating characteristic curve

<sup>a</sup> indicative of AUC comparison between training and testing 1

<sup>b</sup> indicative of AUC comparison between testing 1 and testing 2

<sup>c</sup> indicative of AUC comparison between training and testing 2

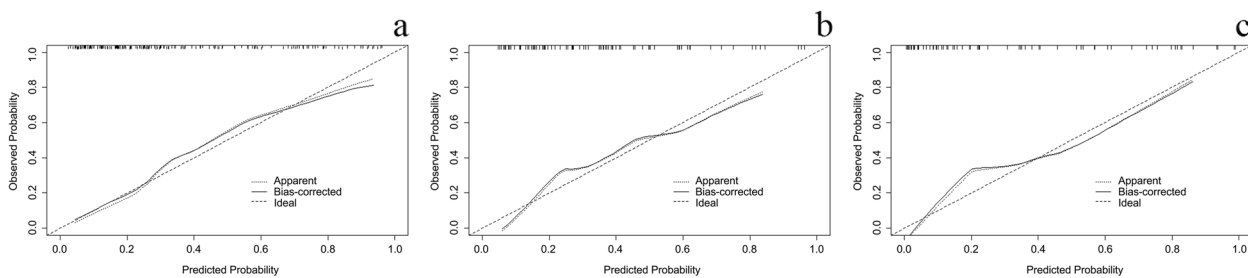


**Fig. 4** Calibration curves of Training, Testing 1 and Testing 2. **a** calibration curves of training, **b** calibration curves of Testing 1, **c** calibration curves of Testing 2

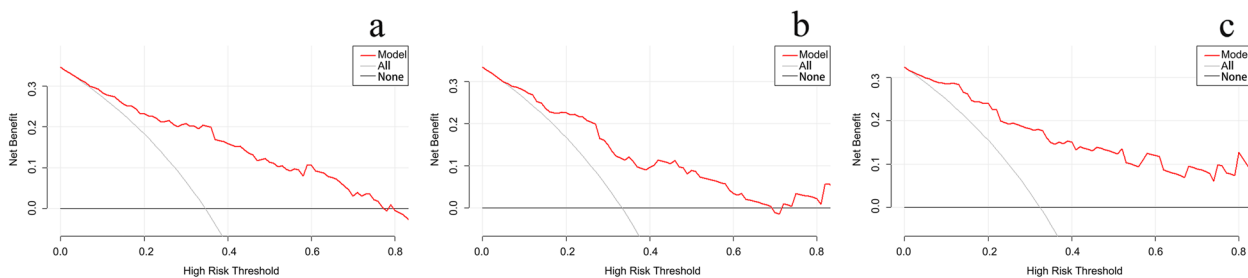


**Fig. 5** Decision curve of Training, Testing 1 and Testing 2. **a** decision curve of Training, **b** decision curve of Testing 1, **c** decision curve of Testing 2

## Abbreviations

HCC	Hepatocellular Carcinoma
MVI	Microvascular Invasion
CT	Computed Tomography
CE-CT	Contrast Enhancement Computed Tomography
DCE-MRI	Dynamic Contrast Enhancement Magnetic Resonance Imaging
AUC	The area under the receiver operating characteristic curves
T2WI	T2-Weighted Imaging
DWI	Diffusion-Weighted Imaging
T1WI	T1-Weighted Imaging
DTPA	Diethylenetriaminepentaacetic Acid
ROC	Receiver Operating Characteristic curve
HBV	Hepatitis B Virus
HCV	Hepatitis C Virus
ALT	Alanine aminotransferase
AST	Aspartate Aminotransferase
ALP	Alkaline Phosphatase
GGT	Glutamyl-transpeptidase
ALB	Albumin
PT	Prothrombin Time
INR	International Normalized Ratio
PLT	Platelet count
TB	Total Bilirubin
AFP	Alpha-fetoprotein
ARE	Arterial Rim Enhancement
APE	Arterial Peritumoral Enhancement
SD	Standard Deviation

## Acknowledgements

The authors would like to express our enormous appreciation and gratitude to all participants.

## Authors' contributions

Study concept and design (Peng Liu, Zhenghan Yang), acquisition of data (Yuhui Deng, Dawei Yang and Xianzheng Tan), analysis and interpretation of data (Peng Liu, Zhenghan Yang, Yuhui Deng, Dawei Yang and Xianzheng Tan), drafting of the manuscript (Dawei Yang, Yuhui Deng), critical revision of the manuscript for important intellectual content (Hui Xu, Ahong Ren, Lixue Xu), administrative, technical, or material support, study supervision (Zhenghan Yang).

## Funding

This work is supported by the National Natural Science Foundation of China (No. 82071876, 82372043, 61871276, 82202266), Beijing Municipal Administration of Hospitals' Youth Programme (No. QML20200108), Changsha Municipal Natural Science Foundation (No. kq2014201), Youth medical key talents foundation of Hunan Province (grant 20230508-1034).

## Availability of data and materials

The datasets used and analysed during the current study are available from the corresponding author upon reasonable request.

## Declarations

### Ethics approval and consent to participate

This study was conformed to the ethical guidelines of the 1964 Declaration of Helsinki as reflected by prior approval from ethical review committee of the Beijing Friendship Hospital of Capital Medical University. All methods were carried out in accordance with relevant guidelines and regulations, waiving the requirement for informed consent because of retrospective study.

### Consent for publication

Not applicable.

### Competing interests

The authors declare no competing interests.

### Author details

<sup>1</sup>Department of Radiology, Beijing Friendship Hospital, Capital Medical University, Yong'an Road 95, West District, Beijing 100050, China. <sup>2</sup>Medical Imaging

Division, Heilongjiang Provincial Hospital, Harbin Institute of Technology, Zhongshan Road 82, Xiangfang District, Harbin 150036, China. <sup>3</sup>Department of Radiology, Hunan Provincial People's Hospital, the First Affiliated Hospital of Hunan Normal University, Changsha 410005, China.

Received: 3 September 2023 Accepted: 18 January 2024

Published online: 27 January 2024

## References

- Golabi P, Fazel S, Otgonsuren M, Sayiner M, Locklear CT, Younossi ZM. Mortality assessment of patients with hepatocellular carcinoma according to underlying disease and treatment modalities. *Medicine (Baltimore)*. 2017;96(9): e5904.
- El-Serag HB. Epidemiology of viral hepatitis and hepatocellular carcinoma. *Gastroenterology*. 2012;142(6):1264-1273.e1.
- Iguchi T, Shirabe K, Aishima S, Wang H, Fujita N, Ninomiya M, et al. New Pathologic Stratification of Microvascular Invasion in Hepatocellular Carcinoma: Predicting Prognosis After Living-donor Liver Transplantation. *Transplantation*. 2015;99(6):1236-42.
- Imamura H, Matsuyama Y, Tanaka E, Ohkubo T, Hasegawa K, Miyagawa S, et al. Risk factors contributing to early and late phase intrahepatic recurrence of hepatocellular carcinoma after hepatectomy. *J Hepatol*. 2003;38(2):200-7.
- Cucchetti A, Piscaglia F, Caturelli E, Benvegnù L, Vivarelli M, Ercolani G, et al. Comparison of recurrence of hepatocellular carcinoma after resection in patients with cirrhosis to its occurrence in a surveilled cirrhotic population. *Ann Surg Oncol*. 2009;16(2):413-22.
- Sumie S, Kuromatsu R, Okuda K, Ando E, Takata A, Fukushima N, et al. Microvascular invasion in patients with hepatocellular carcinoma and its predictable clinicopathological factors. *Ann Surg Oncol*. 2008;15(5):1375-82.
- Oishi K, Itamoto T, Amano H, Fukuda S, Ohdan H, Tashiro H, et al. Clinicopathologic features of poorly differentiated hepatocellular carcinoma. *J Surg Oncol*. 2007;95(4):311-6.
- Deng Y, Li J, Xu H, Ren A, Wang Z, Yang D, et al. Diagnostic Accuracy of the Apparent Diffusion Coefficient for Microvascular Invasion in Hepatocellular Carcinoma: A Meta-analysis. *J Clin Transl Hepatol*. 2022;10(4):642-50.
- Deng Y, Yang D, Xu H, Ren A, Yang Z. Diagnostic performance of imaging features in the HBP of gadoxetate disodium-enhanced MRI for microvascular invasion in hepatocellular carcinoma: a meta-analysis. *Acta radiologica (Stockholm, Sweden: 1987)*. 2022;63(10):1303-14.
- Wei J, Jiang H, Zeng M, Wang M, Niu M, Gu D, et al. Prediction of microvascular invasion in hepatocellular carcinoma via deep learning: a multi-center and prospective validation study. *Cancer*. 2021;131(10):2368.
- Zhang Y, Lv X, Qiu J, Zhang B, Zhang L, Fang J, et al. Deep Learning With 3D Convolutional Neural Network for Noninvasive Prediction of Microvascular Invasion in Hepatocellular Carcinoma. *J magn resonance imaging*. 2021;54(1):134-43.
- Song D, Wang Y, Wang W, Wang Y, Cai J, Zhou K, et al. Using deep learning to predict microvascular invasion in hepatocellular carcinoma based on dynamic contrast-enhanced MRI combined with clinical parameters. *J cancer res clin oncology*. 2021;147(12):3757-67.
- Deng Y, Jia X, Yu G, Hou J, Xu H, Ren A, et al. Can a proposed double branch multimodality-contribution-aware TripNet improve the prediction performance of the microvascular invasion of hepatocellular carcinoma based on small samples? *Front Oncol*. 2022;12:1035775.
- Sacco R, Faggioni L, Bargellini I, Ginanni B, Battaglia V, Romano A, et al. Assessment of response to sorafenib in advanced hepatocellular carcinoma using perfusion computed tomography: results of a pilot study. *Dig Liver Dis*. 2013;45(9):776-81.
- Ippolito D, Pecorelli A, Querques G, Drago SG, Maino C, Franzesi CT, et al. Dynamic computed tomography perfusion imaging: complementary diagnostic tool in hepatocellular carcinoma assessment from diagnosis to treatment follow-up. *Acad Radiol*. 2019;26(12):1675-85.
- Choi JI, Imagawa DK, Bhosale P, Bhargava P, Tirkes T, Seery TE, et al. Magnetic resonance imaging following treatment of advanced hepatocellular carcinoma with sorafenib. *Clin Mol Hepatol*. 2014;20(2):218-22.

17. Ahn SJ, Kim JH, Park SJ, Kim ST, Han JK. Hepatocellular carcinoma: preoperative gadoxetic acid-enhanced MR imaging can predict early recurrence after curative resection using image features and texture analysis. *Abdominal radiol New York*. 2019;44(2):539–48.
18. Zhang L, Yu X, Wei WX, Pan XP, Lu L, Xia JJ, et al. Prediction of HCC microvascular invasion with gadobenate-enhanced MRI: correlation with pathology. *Eur Radiol*. 2020;30(10):5327–36.
19. Renzulli M, Brocchi S, Cucchetti A, Mazzotti F, Mosconi C, Sportoletti C, et al. Can Current Preoperative Imaging Be Used to Detect Microvascular Invasion of Hepatocellular Carcinoma? *Radiology*. 2016;279(2):432–42.
20. Li Y, Xu X, Weng S, Yan C, Chen J, Ye R. CT Image-Based Texture Analysis to Predict Microvascular Invasion in Primary Hepatocellular Carcinoma. *J Digit Imaging*. 2020;33(6):1365–75.
21. Zhang W, Liu L, Wang P, Wang L, Liu L, Chen J, et al. Preoperative computed tomography and serum  $\alpha$ -fetoprotein to predict microvascular invasion in hepatocellular carcinoma. *Med Baltimore*. 2018;97(27):e11402.
22. Uno H, Cai T, Pencina MJ, D'Agostino RB, Wei LJ. On the C-statistics for evaluating overall adequacy of risk prediction procedures with censored survival data. *Statistics med*. 2011;30(10):1105–17.
23. Balachandran VP, Gonen M, Smith JJ. RP DeMatteo Nomograms in oncology: more than meets the eye. *Lancet Oncol*. 2015;16(4):e173–80.
24. Kramer AA, Zimmerman JE. Assessing the calibration of mortality benchmarks in critical care: The Hosmer-Lemeshow test revisited. *Crit care med*. 2007;35(9):2052–6.
25. Vickers AJ, Elkin EB. Decision curve analysis a novel method for evaluating prediction models *Medical decision making*. *Int J Society Med Decis Making*. 2006;26(6):565–74.
26. Zheng J, Chakraborty J, Chapman WC, Gerst S, Gonen M, Pak LM, et al. Preoperative Prediction of Microvascular Invasion in Hepatocellular Carcinoma Using Quantitative Image Analysis. *J Am Coll Surg*. 2017;225(6):778–788.e1.
27. Zhao WC, Fan LF, Yang N, Zhang HB, Chen BD, Yang GS. Preoperative predictors of microvascular invasion in multinodular hepatocellular carcinoma. *Eur J Surg Oncol*. 2013;39(8):858–64.
28. Zhang T, Pandey G, Xu L, Chen W, Gu L, Wu Y, et al. The Value of TTPVI in Prediction of Microvascular Invasion in Hepatocellular Carcinoma. *Cancer Manag Res*. 2020;12:4097–105.
29. McHugh PP, Gilbert J, Vera S, Koch A, Ranjan D, Gedaly R. Alpha-fetoprotein and tumour size are associated with microvascular invasion in explanted livers of patients undergoing transplantation with hepatocellular carcinoma. *HPB (Oxford)*. 2010;12(1):56–61.
30. Shirabe K, Toshima T, Kimura K, Yamashita Y, Ikeda T, Ikegami T, et al. New scoring system for prediction of microvascular invasion in patients with hepatocellular carcinoma. *Liver Int*. 2014;34(6):937–41.
31. Kaibori M, Ishizaki M, Matsui K, Kwon AH. Predictors of microvascular invasion before hepatectomy for hepatocellular carcinoma. *J Surg Oncol*. 2010;102(5):462–8.
32. Ünal E, İdilman İS, Akata D, Özmen MN, Karçaaltıncaba M. Microvascular invasion in hepatocellular carcinoma. *Diagn Interv Radiol*. 2016;22(2):125.
33. Van Zijl F, Mair M, Csiszar A, Schneller D, Zulehner G, Huber H, et al. Hepatic tumor–stroma crosstalk guides epithelial to mesenchymal transition at the tumor edge. *Oncogene*. 2009;28(45):4022–33.
34. Yang L, Gu D, Wei J, Yang C, Rao S, Wang W, et al. A Radiomics Nomogram for Preoperative Prediction of Microvascular Invasion in Hepatocellular Carcinoma. *Liver Cancer*. 2019;8(5):373–86.

## Publisher's Note

Springer Nature remains neutral with regard to jurisdictional claims in published maps and institutional affiliations.